# THE MEASUREMENT OF THE ASYMMETRY OF TENSOR-POLARIZED DEUTERON ELECTRODISINTEGRATION AT 180 MeV ELECTRON ENERGY

M.V. MOSTOVOY, D.M. NIKOLENKO, K.T. OSPANOV, S.G. POPOV, I.A. RACHEK, Yu.M. SHATUNOV, D.K. TOPORKOV, E.P. TSENTALOVICH, B.B. WOITSEKHOWSKI, V.G. ZELEVINSKY
*Institute of Nuclear Physics, Novosibirsk 630090, USSR*

G.A. NAUMENKO and V.N. STIBUNOV
*Nuclear Physics Research Institute, Tomsk 634028, USSR*

Received 15 October 1986

The nucleon emission asymmetry in $\vec{d}$(e, pn)e′ reaction was measured using the tensor-polarized deuterium jet target in the VEPP-2 electron storage ring. At the present experimental accuracy, the results for the proton energy interval $E_p = 12-100$ MeV do not contradict the nonrelativistic calculations.

The structure of two-nucleon systems is a problem of vital interest on the borderline of particle physics and nuclear physics. From the current-day point of view [1], even the understanding of a deuteron as a lightest bound nuclear system is insufficient. One needs both the "classical-type" information (more accurate determination of S- and D-waves of the two-nucleon wave function, especially for high-momentum components, separation of monopole and quadrupole form factors and so on) and the information on a deeper level, namely connected with relativistic effects [2] and with the manifestations of meson exchange currents [3], isobar configurations and subnucleon degrees of freedom.

Polarization experiments, in particular with electromagnetic probes [4–6], could serve as a powerful tool for studying those problems. First polarization measurements [7–9] have been carried out in the elastic (ed) channel with the main goal to determine the quadrupole deuteron form factor. New experiments of the same kind are in progress [10].

Related information can be obtained from the inelastic process of deuteron electro- (or photo-) disintegration. Below we report on the results of the first measurement of the asymmetry in the $\vec{d}$(e, pn)e′ reaction of electrodisintegration of tensor-polarized deuterons by 180 MeV electrons. Like our previous experiments [8,9], the measurement has been performed in the Novosibirsk electron storage ring VEPP-2 using a gas jet of polarized deuterium atoms as an internal target.

Since the main part of the total electrodisintegration cross section is concentrated near small electron scattering angles, the measurement of the energy and the emission angle of the proton is actually sufficient to determine correctly the reaction kinematics in most cases. To extract the events of the process of interest from numerous triggerings of the proton detector, the registration of the proton and the neutron in coincidence was performed. Both time and space p–n correlations were used to identify a pair of nucleons with the disintegration event.

In inelastic electron scattering at small angles the virtual photon absorbed by a deuteron differs only slightly from the real one. Therefore for a qualitative understanding of the main features of the process one may consider the photodisintegration of a tensor-

0370-2693/87/$ 03.50 © Elsevier Science Publishers B.V.
(North-Holland Physics Publishing Division)

polarized deuteron instead of its electrodisintegration. Then in the simplest plane-wave approximation the cross section can be written as follows:

$$\frac{\mathrm{d}\sigma}{\mathrm{d}\Omega_\mathrm{p}} \sim \frac{p\omega}{M}$$

$$\times\left[\left(\frac{p\sin\theta_\mathrm{p}}{\omega}\right)^2 W_\mathrm{e} + \left(\frac{p\sin\theta_\mathrm{p}}{\omega}\right) W_\mathrm{em} + W_\mathrm{m}\right]. \tag{1}$$

Here $\omega$ is the photon energy; $M$, $p$, and $\theta_\mathrm{p}$ are the proton mass, momentum, and emission angle, whereas $W_\mathrm{e}$ and $W_\mathrm{m}$ are proportional to the squared matrix elements of the pure electric and magnetic amplitudes, respectively. $W_\mathrm{em}$ is the interference term. Assuming for simplicity the neutron charge form factor to be zero, one obtains for the main term $W_\mathrm{e}$

$$W_\mathrm{e} = (f_\mathrm{p})^2(F_0^2+8F_2^2)$$

$$\times[1-4P_{zz}P_2((\boldsymbol{n}/n)\cdot\boldsymbol{h})$$

$$\times F_2(F_0+F_2)/(F_0^2+8F_2^2)],$$

$$F_0 = \int_0^\infty j_0(nr)\ u(r) r\,\mathrm{d}r,$$

$$F_2 = \int_0^\infty j_2(nr)\ [w(r)/\sqrt{8}] r\,\mathrm{d}r. \tag{2}$$

Here $P_2$ is a Legendre polynomial, $f_\mathrm{p}$ is the proton charge form factor, $\boldsymbol{n}$ is the momentum of the neutron spectator, $n=|\boldsymbol{n}|$ and $\boldsymbol{h}$ is the unit vector in the direction of the deuteron polarization. The polarization degree is defined by $P_{zz}=1-3b_0$, $b_0$ being the fraction of atoms with the nuclear spin projection $m_z=0$, $F_0$ and $F_2$ are connected with the neutron momentum distributions for S- and D-waves, respectively, $u(r)$ and $w(r)$ are the corresponding wave functions.

It is seen from eqs. (2) that the azimuthal asymmetry with respect to the photon momentum $\boldsymbol{q}$ arises for the nonzero angle between $\boldsymbol{h}$ and $\boldsymbol{q}$. The measurement of this asymmetry taken together with data from unpolarized experiments makes it possible to determine the deuteron inelastic form factors $F_0$ and $F_2$ separately. In a more consistent description taking into account the final state interaction of nucleons, the observed asymmetry can be expressed in a more complicated way in terms of the deuteron bound state and final continuum state wave functions. Therefore the physical information obtainable is richer.

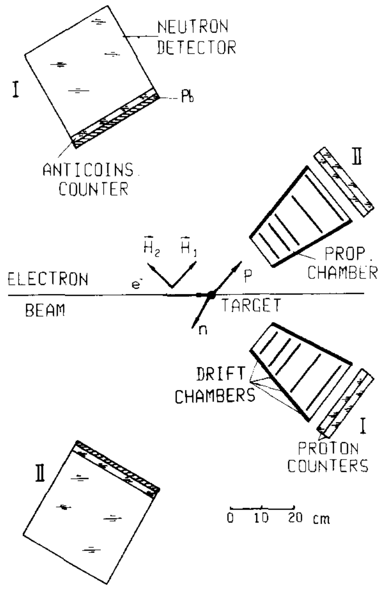


Fig. 1. The experimental scheme for the $\vec{\mathrm{d}}$(e, pn)e′ reaction. I and II correspond to different registration systems, $H_1$ and $H_2$ stand for two directions of the magnetic field fixing the polarization direction.

The experimental arrangement is given schematically in fig. 1. The electron beam with an average current of 0.5 A and a diameter of 5 mm crossed a 7 mm diameter jet of polarized deuterium atoms of about $10^{11}$ at/cm$^2$ thickness. Two identical detection systems, placed symmetrically with respect to the electron beam axis, were used for registration of protons with emission angles $\theta_\mathrm{p}=40°–50°$ and $|\varphi_\mathrm{p}|<10°$ in coincidence with neutrons.

To detect protons, use was made of the electron detectors of the previous experiment [9]. The direction and two coordinates of proton emission were determined by four drift chambers (two nearby wires per cell to remove the left–right ambiguity). The anode voltage of drift chambers has been chosen so as to reduce the efficiency of a chamber with respect to electrons keeping the high registration efficiency

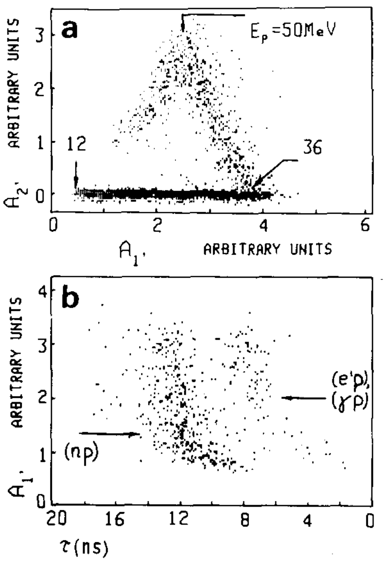


Fig. 2. (a) Event distribution in the $A_1$–$A_2$ plane of the amplitudes for two proton counters. The proton energy is shown for the bending points. (b) Event distribution in the $A_1$–$\tau$ plane ($A_1$ is the amplitude for the first proton counter and $\tau$ is the time interval between signals from the proton and neutron counters).

for protons with $E_p < 100$ MeV. Specific energy losses of particles were measured by proportional chambers.

To determine the proton energy, the amplitudes of signals from two 11 mm thick plastic scintillators were used. The distribution of events in the $A_1$–$A_2$ plane ($A_1$ and $A_2$ being the amplitudes of the counters) is plotted in fig. 2a. The events form a triangle with sharp edges. The proton energies in the vertex points were calculated taking into account the energy losses in the counter material as well as in foils, shields and gas volumes. These energies were used to calibrate the counters. The dependence of the output of light on the specific energy loss was taken into account in the determination of the proton energy.

Neutrons were registered by 300 mm diameter plastic scintillators with an efficiency of about 20–30%. Neutron counters were preceded by anticoincidence counters and 10 mm thick lead converters to reduce the photon background. The distance between the neutron counters and the target was equal to 60 cm.

The deuteron disintegration events were discriminated using the relation between $E$ and $dE/dX$ in proton detection systems, the coordinate of proton emission from the target region and the time interval $\tau$ between triggerings of proton and neutron counters.

Fig. 2b shows the event distribution in the $A_1$–$\tau$ plane. One can see the points corresponding to the events with $A_2=0$ (e.g. the proton stops in the first counter) and without a signal from the anticoincidence counter. It is obvious that the time resolution permits one to separate the background coincidences of a proton with fast particles. Such background events may happen, for instance, from the d(e, $\pi^0$p)e′n process as well as from the proton quasielastic knockout d(e, e′p)n if for some reasons there was no anticoincidence counter signal.

The experiment was carried out at four different states of target polarization. The polarization direction as well as the type of the radio-frequency transition between h.f.s. states determining the sign of $P_{zz}$ were changed each 5–6 min during the 125 h data taking period. The polarization direction was fixed by a magnetic field of 0.37 kG being oriented alternatively at $\theta_h=40°$ and 130° ($H_1$ and $H_2$ directions correspondingly, see fig. 1).

The degree of the tensor polarization of a gas jet ($|P_{zz}|$), was determined from the analysis of the deviations of atoms in a nonuniform magnetic field [11]. Such measurements were repeated many times during the experiment.

The average $P_{zz}$ values are equal to $0.92\pm0.09$ and $-0.84\pm0.11$ for different rf transitions. Note that rf transitions devastating the substate with $m_z=0$ ($P_{zz}>0$) have a higher probability. The spread of $P_{zz}$ values is, to some extent, due to measurement errors. It is confirmed by the fact that in some measurements values of $|P_{zz}|>1$ were obtained, which is impossible for the utilized types of rf transitions. However, we below identify this spreading with an error on the value of $P_{zz}$.

The effective degree of deuterium polarization $P_{zz}^{\rm eff}$ in the intersection region of the gas jet with the electron beam is less than $P_{zz}$. It is reduced because of (i) the finite value of the governing field (the corresponding correction factor is $C_1=0.934$) and (ii) the nonpolarized target background. To determine the unpolarized background use was made of the distribution of events with respect to the coordinate $X$ of proton emission from the target region along the electron beam axis. The corresponding histogram of events are plotted in fig. 3. The upper histogram was obtained with the target switched on whereas the

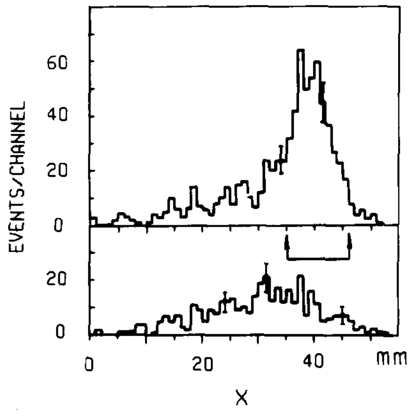


Fig. 3. Histogram with respect to the $X$ coordinate of proton emission from the target region. The upper histogram corresponds to the target switched on whereas the lower one corresponds to the target switched off at the increased deuterium concentration in the vacuum chamber of the storage ring. Arrows indicate the $X$ range covering the target location.

lower one is for the target switched off when the deuterium concentration in the vacuum chamber of the storage ring is known.

Assuming the same shape of the distribution of background events for both histograms we found the polarization correction factor $C_2=0.73\pm0.04$ for events from the interval of $X$ which contains the target (see fig. 3). Finally, we have that $P_{zz}^{\text{eff}}=P_{zz}C_1C_2$ is equal to $0.63\pm0.07$ or $-0.57\pm0.08$ correspondingly, for two types of rf transitions.

The high level of the nonpolarized background does not correspond to the deuterium partial pressure ($10^{-8}$ Torr) established in the vacuum chamber when the target is switched on. It can be explained by the effect of ion confinement in the electrostatic field of the electron beam, assuming the complete compensation of the beam charge by deuterium ions alone. The nonlinear dependence of the p–n coincidence counting rate on the deuterium pressure in the chamber when the target is switched off can be regarded as a confirmation of such an explanation. For pressures of $2\times10^{-8}$ Torr and $2\times10^{-6}$ Torr the counting rates differ by one order of magnitude only, rather than by two orders, so just the ion confinement determines the counting rate at small pressure.

Let us denote the counting rate of the first system as $R^{\text{I}}_{1+}$ for the case when $P_{zz}>0$ and the direction of the polarization is fixed by the magnetic field $\boldsymbol{H}_1$ (see fig. 1). Here and below the upper index labels the detection system while the lower one coincides with the field index in the notation $\boldsymbol{H}_i$ and the sign index is simply the sign of $P_{zz}$. According to eq. (2), $R^{\text{I}}_{1+}$ should exceed the similar quantity $R^{\text{II}}_{1+}$ for the second system at the same polarization state of a target. The situation reverses when the sign of $P_{zz}$ or the direction of the magnetic field are changed. Therefore we define the average cross section asymmetry for the four polarization states of a target as follows:

Table 1
The asymmetry of the $\vec{\text{d}}$(e, pn)e′ reaction cross section.

| $E_{\text{p}}$ [MeV] | $\omega$ [MeV] | $n$ [MeV/$c$] | $\alpha$ (×100) |
|---|---|---|---|
| 12– 24 | 22– 44 | 135–185 | 8.9± 4.7 |
| 24– 36 | 44– 64 | 185–222 | 19.2± 5.7 |
| 36– 50 | 64– 86 | 222–257 | 18.1±10.2 |
| 50–100 | 86–164 | 257–348 | 42.4±11.6 |

$$a=\frac{1}{4}\left(\frac{R^{\text{I}}_{1+}-R^{\text{II}}_{1+}}{R^{\text{I}}_{1+}+R^{\text{II}}_{1+}}-\frac{R^{\text{I}}_{1-}-R^{\text{II}}_{1-}}{R^{\text{I}}_{1-}+R^{\text{II}}_{1}}\right.$$

$$\left.-\frac{R^{\text{I}}_{2+}-R^{\text{II}}_{2+}}{R^{\text{I}}_{2+}+R^{\text{II}}_{2+}}+\frac{R^{\text{I}}_{2-}-R^{\text{II}}_{2-}}{R^{\text{I}}_{2-}+R^{\text{II}}_{2-}}\right). \quad (3)$$

Note that the asymmetry, defined according to eq. (3), is insensitive, in the first approximation, to the systematic errors due to the difference of the efficiencies and the solid angles of the detectors.

The values of asymmetry measured for the different regions of the proton energy $E_{\text{p}}$ are listed in table 1 and plotted in fig. 4. The energy transfer $\omega$ and the neutron momentum $n$ in the table are calculated for the two-body break-up of a deuteron, and the electron scattering angle $\theta_{\text{e}}=0°$.

The averaged asymmetry (multiplied by 100) for the events from the tail of the $X$-distribution (the upper histogram in fig. 3) and for the events obtained at the switched-off target with a deuterium pressure in the vacuum chamber of $2\times10^{-6}$ Torr is equal to $-2.0\pm4.3$ and $0.6\pm3.5$, respectively, e.g. within the error bars it is zero.

Fig. 4 shows the experimental points together with theoretical predictions. Curve 1 is the result of a calculation in the plane-wave approximation for the final state using the Hamada–Johnston potential for the bound initial state. One can naturally ascribe the

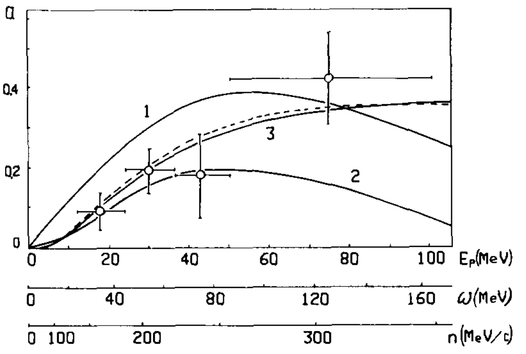


Fig. 4. The cross section asymmetry (see eq. (3) in the text) for the $\vec{d}$(e, pn)e′ reaction of the disintegration of the tensor-polarized deuteron. Experimental data are shown by dots with error bars. The curves are theoretical results for: the final state plane wave approximation with the Hamada–Johnston initial bound wave function (curve 1); the relativistic impulse approximation with the RSC potential (calculations by the authors of ref. [6] according to the method of that reference) (curve 2); the nonrelativistic calculation by H. Arenhövel with the final state interaction effects [12] for the RSC potential (curve 3), the dashed curve corresponds to the addition of meson exchange currents and isobar excitations. $E_p$ is the proton energy, $\omega$ is the transfer energy and $n$ is the neutron momentum.

excess of the predicted asymmetry compared with the experimental one for small proton energies to the final state p–n interaction. Curve 2 is obtained by the calculation in the relativistic impulse approximation [6] using the deuteron wave function from the Reid soft core (RSC) potential. Here the final state interaction is partially taken into account (in the channel with the deuteron quantum numbers). These results agree with experiment for small $E_p$, but underestimate the asymmetry for $E_p \sim 80$ MeV.
Finally, curve 3 represents the results of a consistent nonrelativistic calculation [12] also using the RSC potential with the final state interaction taken into account exactly. The dashed line includes, in addition, the contribution of mesonic exchange currents and isobar excitations [12]. Experimental data are reasonably described by these curves. The improvement of the accuracy of the experiment will give the possibility to discriminate distinctly between different theoretical models.

We would like to thank H. Arenhövel, G.I. Gakh and A.P. Rekalo for their interest in our work and for the performing of calculations adapted to the experimental kinematics. We appreciate the useful discussions with V.F. Dmitriev, M.I. Strikman and M.P. Rekalo.

*References*


[1] R.G. Arnold, C.E. Carlson and F. Gross, Phys. Rev. C 21 (1980) 1426; C 23 (1981) 363.
[2] L.L. Frankfurt and M.I. Strikman, Phys. Rep. 76 (1981) 717.
[3] H. Arenhövel, Nucl. Phys. A 358 (1981) 263.
[4] M.I. Strikman and L.L. Frankfurt, Yad. Fiz. 38 (1983) 239, 339.
[5] C.Y. Cheung and R.M. Voloshyn, Phys. Lett. B 127 (1983) 147.
[6] M.P. Rekalo, G.I. Gakh and A.P. Rekalo, Phys. Lett. B 166 (1986) 27.
[7] M.E. Shulze et al., Phys. Rev. Lett. 52 (1984) 597.
[8] V.F. Dmitriev et al., Phys. Lett. B 157 (1985) 143.
[9] B.B. Woitsekhowski et al., JETP Lett. 43 (1986) 567.
[10] Nuclear physics with electromagnetic probes, XI Europhys. Divisional Conf. (Paris, July 1985).
[11] A.V. Evstigneev, S.G. Popov and D.K. Toporkov, Nucl. Instrum. Methods A 238 (1985) 12.
[12] H. Arenhövel, private communication.